JACS
JOURNAL OF THE AMERICAN CHEMICAL SOCIETY

Communication

pubs.acs.org/JACS

Template-Free Synthesis of Hierarchical Porous Metal–Organic Frameworks

Yanfeng Yue,*[,†] Zhen-An Qiao,[†] Pasquale F. Fulvio,[†] Andrew J. Binder,[‡] Chengcheng Tian,[‡] Jihua Chen,[§] Kimberly M. Nelson,[‡] Xiang Zhu,[‡] and Sheng Dai*[,†,‡]

[†]Chemical Sciences Division, Oak Ridge National Laboratory, Oak Ridge, Tennessee 37831, United States

[‡]Department of Chemistry, University of Tennessee, Knoxville, Tennessee 37996, United States

[§]Center for Nanophase Materials Sciences, Oak Ridge National Laboratory, Oak Ridge, Tennessee 37831, United States

Supporting Information

ABSTRACT: A template-free synthesis of a hierarchical microporous–mesoporous metal–organic framework (MOF) of zinc(II) 2,5-dihydroxy-1,4-benzenedicarboxylate (Zn-MOF-74) is reported. The surface morphology and porosity of the bimodal materials can be modified by etching the pore walls with various synthesis solvents for different reaction times. This template-free strategy enables the preparation of stable frameworks with mesopores exceeding 15 nm, which was previously unattained in the synthesis of MOFs by the ligand-extension method.

The field of mesoporous materials with a well-defined pore size has grown at a fast pace over the last decades because of the various applications found for these materials.[1] In contrast, the investigation of crystalline metal–organic frameworks (MOFs) with a hierarchical structure of micropores and mesopores is still in its infancy, and the augmentation of their channel sizes to the mesoporous range (2–50 nm) still poses great challenges.[2]

MOFs are hybrid inorganic–organic crystalline solids formed by the linking of single metal ions or metal clusters with tunable oligotopic organic ligands. In particular, this new class of porous materials has attracted a tremendous amount of interest because of their fascinating structural topologies and potential uses in gas storage, gas separation, catalysis, and sensing.[3−5] Almost all of the MOFs reported to date are microporous (pore sizes <2 nm). Such small pores can restrict diffusion of gaseous and reactive species and prevent large molecules from accessing the active metal centers within the bulk of the MOF, thus limiting their application.

To expand the pore widths of MOFs, the ligand-extension method, which involves the use of longer organic ligands, has been demonstrated.[6] However, the periodic nanostructure or pores could be retained only for small mesopore sizes, or constricted cages resulted from this method.[7] In addition, ligand extension also resulted in the collapse of the open MOF pores in the absence of guest molecules. Hence, other methods had to be developed in order to prepare MOFs with stable mesopores.

Mesoporous MOFs have also been prepared in the presence of surfactants using a method similar to that previously reported for the synthesis of various mesoporous metal oxides and silicas.[2a−e] The mesoporous MOFs obtained through this cooperative template method contain a surfactant along with the organic ligands,[8] which requires additional steps to remove the template, thus adding difficulties in retaining the mesopores. Hence, the development of template-free and facile methods to make mesoporous crystalline MOFs are of great interest for their large-scale preparation and applications.

Herein we demonstrate a surfactant-free methodology for the template-free room-temperature synthesis of Zn-MOF-74, a hierarchical microporous–mesoporous MOF having the formula $Zn_2(DHBDC)\cdot(guest)_n$ (DHBDC = 2,5-dihydroxy-1,4-benzenedicarboxylate). In a typical synthesis of a mesoporous Zn(II)–DHBDC framework, zinc acetate and H_2DHBDC were dissolved in *N*,*N*-dimethylformamide (DMF) [see the Supporting Information (SI)]. The mixture was then stirred for various reaction times at room temperature, and the product was subsequently separated by centrifugation and washed with DMF and methanol. The materials were labeled as Zn-MOF-74/*t*, in which *t* stands for the reaction time in hours. Hierarchical Zn-MOF-74/*t* materials could be prepared with as little as 15 min of stirring at room temperature, in contrast to the coassembly process of nanosized building blocks and surfactant micelles, for which the growth of the framework must be slow enough to avoid phase separation. When the starting zinc acetate was replaced by zinc chloride, zinc nitrate, or zinc sulfate salts, only clear solutions were obtained under same reaction conditions. For comparison, a standard microporous Zn-MOF-74 was prepared according to a previously reported solvothermal synthesis.

The mesostructure of bimodal Zn-MOF-74 was revealed by scanning electron microscopy (SEM) and transmission electron microscopy (TEM). As observed in the SEM image (Figure 1a), continuous networks of Zn-MOF-74 particles were formed. Disordered mesopores with widths of 5–20 nm were formed between these particles, as shown in the TEM image (Figure 1b). SEM images of dry Zn-MOF-74/18 also showed a similar mesostructure with a network morphology, indicating that the structure was retained after heating at 150 °C under flowing nitrogen (Figure S1 in the SI). In thermogravimetric analysis (TGA), this hierarchical microporous–mesoporous material exhibited a weight change below 200 °C associated with the loss of solvent guest molecules (Figure S2). The greater decom-

Received: March 16, 2013
Published: June 19, 2013

   dx.doi.org/10.1021/ja402694f | J. Am. Chem. Soc. 2013, 135, 9572–9575

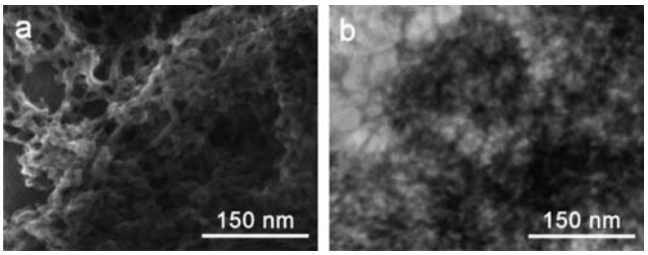

Figure 1. (a) SEM and (b) TEM images of the bimodal microporous–mesoporous material Zn-MOF-74/18.

position step above 300 °C corresponds to the decomposition of the organic ligands used. The relatively high thermal decomposition temperature shows that Zn-MOF-74/*t* has good thermal stability properties.

The hierarchical Zn-MOF-74/*t* materials prepared with different reaction times were crystalline but exhibited broader powder X-ray diffraction (XRD) peaks than in the simulated XRD pattern of a single crystal or the pattern for the microporous Zn-MOF-74 reference material (Figure S3). The XRD patterns for the mesoporous materials were further compared with the simulated pattern of the single crystal, where additional reflections indicated the presence of other unidentified phases present in the Zn-MOF-74/*t* and Zn-MOF-74 samples (Figure S3). Furthermore, nanocrystalline Zn-MOF-74 samples were prepared with other polar aprotic solvents, including *N*,*N*-dimethylacetamide (DMA) and *N*-methylpyrrolidone (NMP), and they exhibited morphologies and pore structures similar to those of the materials prepared in DMF (see the XRD patterns and SEM and TEM images in Figures S4 and S5). However, crystalline phases were not obtained using water or methanol as the solvent.

Five members of the Zn-MOF-74 series obtained with different reaction times all exhibited accessible porosity, as confirmed by N_2 adsorption–desorption isotherms (Figure 2).

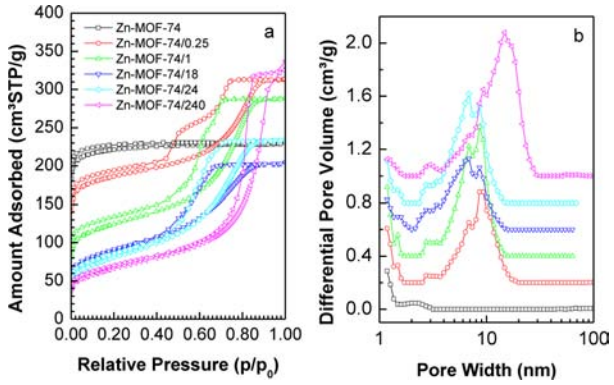

Figure 2. (a) N_2 isotherms at −196 °C and (b) corresponding pore size distributions (PSDs) calculated by NLDFT assuming a slitlike pore geometry for the microporous Zn-MOF-74 and bimodal Zn-MOF-74/*t* samples. For clarity, the PSDs have been vertically offset in increments of 0.2 cm^3/g.

Prior to the gas sorption measurements, lattice guest molecules were removed by solvent exchange followed by thermal activation at 150 °C under flowing N_2. In contrast to the type-I isotherm for the microporous Zn-MOF-74, type-IV isotherms with hysteresis loops characteristic of large constricted mesopores were observed for all of the Zn-MOF-74/*t* samples (Figure 2a).[9] Furthermore, for the Zn-MOF-74/0.25 and Zn-MOF-74/1 samples, a second desorption step indicative of additional constrictions was observed. In general, such large constricted pores form between aggregates of microporous particles. The pore-size distribution (PSD) of the micropores in Zn-MOF-74/1 was calculated using nonlocal density functional theory (NLDFT) assuming a cylindrical pore geometry and compared with that of Zn-MOF-74 (Figure S6). While the gas uptake at low relative pressure (p/p_0) was significantly lower than for the microporous reference solid (Figure S6a), the calculated PSDs revealed distributions of micropores for both materials with maxima at ∼1.1 nm, in good agreement with the results of single-crystal XRD analysis.[3g] Moreover, the mesopore width was as large as 9 nm in Zn-MOF-74/0.25 (Figure 2b and Table S1 in the SI). The maximum of the PSD indicated that the mesopores were finally enlarged to nearly 15 nm in the case of Zn-MOF-74/240. The specific surface area systematically decreased as the ratio of the micropore volume to the total pore volume (from the α_S-plot analysis) decreased (Table S1). The latter result indicates that the fraction of mesopores increased at the expense of a decrease in the fraction of microporous particles in the framework walls (Table S1). At very long reaction times, as for Zn-MOF-74/240, the mesopores were greatly enlarged and the micropore volume reached its minimum value. Finally, the adsorptive and structural properties of these materials were also influenced by postsynthesis hydrothermal treatments. For instance, after Zn-MOF-74/18 was heated in water for 6 h at 150 °C using an autoclave, the crystallite sizes were larger than 100 nm (Figure S1). In addition, the micropore volume increased from 0.03 to ∼0.18 cm^3/g, and the specific surface area increased by ∼100 m^2/g. Also, the shape of the adsorption isotherm after hydrothermal treatment (not shown) largely resembled that of the microporous material but had a condensation step above p/p_0 = 0.9. The latter indicated that upon recrystallization of the pore walls into large microporous particles, the textural mesopores were converted into very large mesopores and small macropores (>50 nm).

SEM images showed that relatively larger particles built up the framework of Zn-MOF-74/240. However, the broadening of the powder XRD peaks of the products after long reaction times further suggested that the MOF crystals forming the pore walls were smaller or had a lower degree of periodicity (Figure S3 and Table S1). The calculated crystallite sizes for the other materials decreased by ∼2 nm in going from Zn-MOF-74/0.15 to Zn-MOF-74/24. Furthermore, the lowest number of micropores was found for Zn-MOF-74/240, for which the smallest crystallites (8.9 nm) were observed. Hence, the smaller crystallites must be interconnected by residual material with a considerably lower degree of periodicity and lower micropore volume. This was also supported by high-resolution TEM (HRTEM), as shown in Figure 3 for Zn-MOF-74/18. Lattice fringes were observed for some of the aggregated particles, but particles having disordered structures were also present. The spacing of such fringes varied from 0.7 to 2.0 nm. The sensitivity of this material to the electron beam prevented the observation of more lattice fringes.

On the basis of the above results and literature precedents, a possible mechanism for the formation of bimodal porous Zn-MOF-74 is summarized in Scheme 1. In the initial stages of the reaction between the Zn precursors and ligands at room temperature, the bidentate-acetate-bridged $[Zn_2(CH_3COO)_4]$ units form.[8b,10] Upon the addition of the ligand precursor H_2DHBDC, nanosized MOF-74 crystals precipitate in addition

dx.doi.org/10.1021/ja402694f | J. Am. Chem. Soc. 2013, 135, 9572–9575

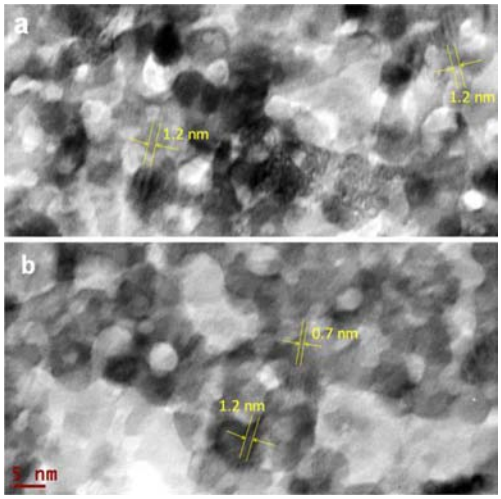

Figure 3. HRTEM images of Zn-MOF-74/18 showing two regions of the same sample. In addition to the textural pores, lattice fringes (highlighted in yellow) were seen for several particles. Amorphous and less-periodic particles were also present. The scale bar in (b) applies to both images.

Scheme 1. Schematic Illustration of a Possible Mechanism for the Formation of the Bimodal Microporous–Mesoporous MOF Material and the Morphology Transformation by Solvent Etching (I–III)

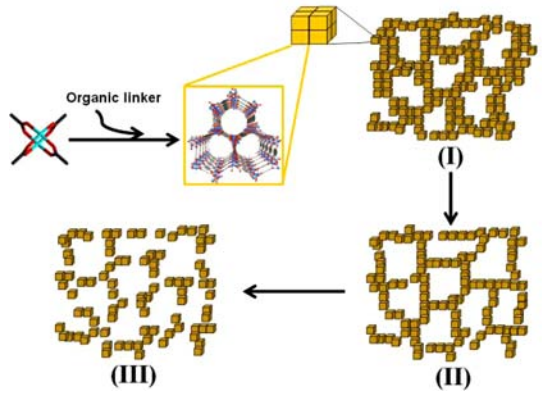

to amorphous metal complexes, since the organic linkers compete with the carboxylate bridging ligands. At this stage, the formation of nanosized MOF-74 crystals possibly occurs via deprotonation of the linker precursors by the acetate groups. The latter process would not be expected to happen with the conjugate bases of strong acids (e.g., Cl^-, SO_4^{2-}, and NO_3^-). Thus, the acetate accelerates the MOF crystal formation through a ligand-exchange process.[11] The precipitated material is composed of discrete nanosized Zn-MOF-74 particles embedded in an amorphous matrix. The latter exhibits thick pore walls and large mesopores formed between particle aggregates (Figure 4a). The high micropore volume of 0.22 cm^3/g for the sample obtained after a short reaction time provides evidence of the large quantities of crystalline particles forming the pore walls in comparison with amorphous compounds. When the synthesis time is extended to 1 h, the solvent bearing a ketone functional group partially etches the crystalline pore walls and induces recrystallization of a less-ordered crystal lattice. This leads to a 60% decrease in microporosity, whereas the pore walls are still relatively thick (Figure 4b) and the mesopore widths still lie

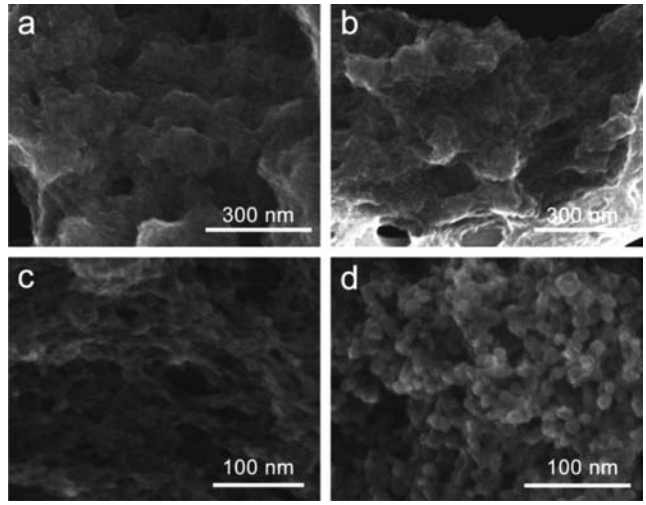

Figure 4. SEM images for bimodal Zn-MOF-74 series synthesized with different reaction time (a) 0.25 h, (b) 1 h, (c) 24 h, and (d) 240 h.

within the 6–8 nm range. Upon further stirring of the precipitate, the etching of the crystalline framework proceeds, systematically reducing the micropore volume and increasing the number of mesopores (Figure 4c). After 10 days, this process is even more pronounced, and the resulting Zn-MOF-74/240 material has almost discrete interconnected particles (Figure 4d). The latter are less crystalline and consequently exhibit ~10% of the micropore volume of Zn-MOF-74/0.25 along with the largest mesopore width and mesopore volume (0.48 cm^3/g).

The effect of other solvents (DMA and NMP) on the MOF structure and porosity was also verified (Table S1 and Figures S4, S5, and S7). After 18 h of reaction time, smaller crystals were obtained in the mesoporous Zn-MOF-74 materials prepared from DMA and NMP than in those prepared in DMF. The smallest crystallites (~6.5 nm) were obtained in NMP (Table S1). The latter sample also exhibited slightly larger mesopores and higher mesopore volume than Zn-MOF-74/18-DMA. Hence, in addition to the reaction time, the adsorption and structural parameters are influenced by solvent.[12]

To assess the improvement in the adsorption capacity of these hierarchical porous materials, a dye uptake study was performed using a large dye molecule, Brilliant Blue R-250 (BBR-250), with Zn-MOF-74/18 or microporous Zn-MOF-74 as the sorbent. The adsorption study was conducted by soaking freshly made sorbent materials in concentrated methanol solutions of BBR-250, which has molecular dimensions of ~1.8 nm × 2.2 nm,[13] making it larger than the microporous cavities of standard Zn-MOF-74. After separation of the saturated solid materials, UV–vis analysis showed that the supernatant solutions contained different amounts of BBR-250 (Figure S8): Zn-MOF-74/18 adsorbed 17.9%, in contrast to only 2.7% adsorbed by microporous Zn-MOF-74. The observed results can only be explained by the presence of mesopores in Zn-MOF/18, whereas the dye probably adsorbed on the small external surfaces of Zn-MOF-74. The remarkable difference in the dye uptake abilities of the bimodal and microporous MOF materials indicates that the additional mesopores allow large molecules in solution to access less coordinately saturated surface metal centers.[14]

In summary, a facile template-free synthesis of hierarchical microporous–mesoporous Zn-MOF-74 materials is reported. Materials having nanocrystalline pore walls, high surface areas, and large mesopores were obtained after as little as 15 min of

dx.doi.org/10.1021/ja402694f | J. Am. Chem. Soc. 2013, 135, 9572–9575

reaction at room temperature. The morphology of the material varied with reaction time, from rugged smooth surfaces formed by large crystallites to interconnected small MOF particles. Finally, the crystallinity and the adsorption properties of these materials could also be controlled by using different solvents. Compared with their microporous MOF-74 counterparts, this hierarchical crystalline Zn-MOF-74 is of great scientific and technological interest because of its ability to transport guest molecules larger than the microporous cavities of Zn-MOF-74. Short diffusion pathways resulting from the textural mesopores and the more exposed metal coordination sites make these potential materials for applications in separations, drug delivery, heterogeneous catalysis, and sensing.

■ ASSOCIATED CONTENT

Supporting Information

Synthesis and characterization of hierarchical micromesoporous MOFs; SEM image and powder XRD patterns of Zn-MOF-74/18 after thermal and hydrothermal treatments; TGA curve for Zn-MOF-74/18; powder XRD patterns of the Zn-MOF-74 series obtained after different reaction times; powder XRD patterns and SEM and TEM images of Zn-MOF-74 series obtained with different solvents; summary of calculated adsorption parameters of Zn-MOF-74 materials obtained with different reaction times; N_2 adsorption−desorption isotherms of bimodal Zn-MOF-74 materials obtained with different solvents; and UV−vis spectra of BBR-250 methanol solutions in which the MOF materials were soaked for 24 h. This material is available free of charge via the Internet at http://pubs.acs.org.

■ AUTHOR INFORMATION

Corresponding Author

yuey@ornl.gov; dais@ornl.gov

Notes

The authors declare no competing financial interest.

■ ACKNOWLEDGMENTS

This research was sponsored by the Division of Chemical Sciences, Geosciences, and Biosciences, Office of Basic Energy Sciences, U.S. Department of Energy, under Contract DE-AC05-00OR22725 with Oak Ridge National Laboratory, which is managed and operated by UT-Battelle, LLC. A portion of this research was conducted at the Center for Nanophase Materials Sciences, which is sponsored at Oak Ridge National Laboratory by the Division of Scientific User Facilities, Office of Basic Energy Sciences, U.S. Department of Energy.

■ REFERENCES

(1) (a) Wan, Y.; Zhao, D. *Chem. Rev.* **2007**, *107*, 2821. (b) Polarz, S.; Orlov, A. V.; Schüth, F.; Lu, A.-H. *Chem.—Eur. J.* **2007**, *13*, 592. (c) Wang, X.; Liang, C.; Dai, S. *Langmuir* **2008**, *24*, 7500. (d) Liu, F.; Kong, W.; Qi, C.; Zhu, L.; Xiao, F. *ACS Catal.* **2012**, *2*, 565. (e) Zhao, D.; Huo, Q.; Feng, J.; Chmelka, B. F.; Stucky, G. D. *J. Am. Chem. Soc.* **1998**, *120*, 6024. (f) Yang, C.-M.; Lin, H.-A.; Zibrowious, B.; Spliethoff, B.; Schüth, F.; Liou, S.-C.; Chu, M.-W.; Chen, C.-H. *Chem. Mater.* **2007**, *19*, 3205. (g) Huo, Q.; Margolese, D. I.; Ciesla, U.; Demuth, D.; Feng, P.; Gier, T. E.; Sieger, P.; Firouzi, A.; Chmelka, B. F. *Chem. Mater.* **1994**, *6*, 1176.

(2) (a) Qiu, L.-G.; Xu, T.; Li, Z.-Q.; Wang, W.; Wu, Y.; Jiang, X.; Tian, X.-Y.; Zhang, L.-D. *Angew. Chem., Int. Ed.* **2008**, *47*, 9487. (b) Zhao, Y.; Zhang, J.; Han, B.; Song, J.; Li, J.; Wang, Q. *Angew. Chem., Int. Ed.* **2011**, *50*, 636. (c) Peng, L.; Zhang, J.; Li, J.; Han, B.; Xue, Z.; Yang, G. *Chem. Commun.* **2012**, *48*, 8688. (d) Choi, M.; Cho, H. S.; Srivastava, R.; Venkatesan, C.; Choi, D.-H.; Ryoo, R. *Nat. Mater.* **2006**, *5*, 718. (e) Górka, J.; Fulvio, P. F.; Pikus, S.; Jaroniec, M. *Chem. Commun.* **2010**, *46*, 6798. (f) Xin, Z.; Bai, J.; Pan, Y.; Zaworotko, M. J. *Chem.—Eur. J.* **2010**, *16*, 13049.

(3) (a) D'Alessandro, D. M.; Smit, B.; Long, J. R. *Angew. Chem., Int. Ed.* **2010**, *49*, 6058. (b) Yaghi, O. M.; O'Keeffe, M.; Ockwig, N. W.; Chae, H. K.; Eddaoudi, M.; Kim, J. *Nature* **2003**, *423*, 705. (c) Ma, L.; Abney, C.; Lin, W. *Chem. Soc. Rev.* **2009**, *38*, 1248. (d) Cui, Y.; Yue, Y.; Qian, G.; Chen, B. *Chem. Rev.* **2012**, *112*, 1126. (e) Wang, Z.; Cohen, S. M. *Chem. Soc. Rev.* **2009**, *38*, 1315. (f) Shimizu, G. K. H.; Vaidhyanathan, R.; Taylor, J. M. *Chem. Soc. Rev.* **2009**, *38*, 1430. (g) Rosi, N. L.; Kim, J.; Eddaoudi, M.; Chen, B.; O'Keeffe, M.; Yaghi, O. M. *J. Am. Chem. Soc.* **2005**, *127*, 1504.

(4) (a) Furukawa, S.; Hirai, K.; Takashima, Y.; Nakagawa, K.; Kondo, M.; Tsuruoka, T.; Sakata, O.; Kitagawa, S. *Chem. Commun.* **2009**, 5097. (b) Khlobystov, A. N.; Blake, A. J.; Champness, N. R.; Lemenovskii, D. A.; Majouga, A. G.; Zyk, N. V.; Schröder, M. *Coord. Chem. Rev.* **2001**, *222*, 155. (c) Farha, O. K.; Wilmer, C. E.; Eryazici, I.; Hauser, B. G.; Parilla, P. A.; O'Neill, K.; Sarjeant, A. A.; Nguyen, S. T.; Snurr, R. Q.; Hupp, J. T. *J. Am. Chem. Soc.* **2012**, *134*, 9860. (d) Moulton, B.; Zaworotko, M. J. *Chem. Rev.* **2001**, *101*, 1629. (e) Li, J. R.; Kuppler, R.-J.; Zhou, H.-C. *Chem. Soc. Rev.* **2009**, *38*, 1477.

(5) (a) Bourrelly, S.; Llewellyn, P. L.; Serre, C.; Millange, F.; Loiseau, T.; Férey, G. *J. Am. Chem. Soc.* **2005**, *127*, 13519. (b) Ben, T.; Lu, C. J.; Pei, C. Y.; Xu, S. X.; Qiu, S. L. *Chem.—Eur. J.* **2012**, *18*, 10250. (c) Zhang, J. P.; Zhang, Y. B.; Lin, J. B.; Chen, X. M. *Chem. Rev.* **2012**, *112*, 1001. (d) Asta, M.; Laird, B. B.; Yaghi, O. M. *J. Am. Chem. Soc.* **2010**, *132*, 11006. (e) Cliffe, M. J.; Mottillo, C.; Stein, R. S.; Bučar, D. K.; Friščić, T. *Chem. Sci.* **2012**, *3*, 2495. (f) Zheng, S. T.; Wu, T.; Chou, C. T.; Fuhr, A.; Feng, P. Y.; Bu, X. H. *J. Am. Chem. Soc.* **2012**, *134*, 1934.

(6) (a) Deng, H.; Grunder, S.; Cordova, K. E.; Valente, C.; Furukawa, H.; Hmadeh, M.; Gándara, F.; Whalley, A. C.; Liu, Z.; Asahina, S.; Kazumori, H.; O'Keeffe, M.; Terasaki, O.; Stoddart, J. F.; Yaghi, O. M. *Science* **2012**, *336*, 1018. (b) Lykourinou, V.; Chen, Y.; Wang, X.-S.; Meng, L.; Hoang, T.; Ming, L.-J.; Musselman, R. L.; Ma, S. *J. Am. Chem. Soc.* **2011**, *133*, 10382. (c) Liu, C.; Li, T.; Rosi, N. L. *J. Am. Chem. Soc.* **2012**, *134*, 18886. (d) Klein, N.; Senkovska, I.; Gedrich, K.; Stoeck, U.; Henschel, A.; Mueller, U.; Kaskel, S. *Angew. Chem., Int. Ed.* **2009**, *48*, 9954. (e) Sonnauer, A.; Hoffmann, F.; Fröba, M.; Kienle, L.; Duppel, V.; Thommes, M.; Serre, C.; Férey, G.; Stock, N. *Angew. Chem., Int. Ed.* **2009**, *48*, 3791.

(7) (a) Yang, S.; Lin, X.; Lewis, W.; Suyetin, M.; Bichoutskaia, E.; Parker, J. E.; Tang, C. C.; Allan, D. R.; Rizkallah, P. J.; Hubberstey, P.; Champness, N. R.; Thomas, K. M.; Blake, A. J.; Schröder, M. *Nat. Mater.* **2012**, *11*, 710. (b) Thallapally, P. K.; Tian, J.; Kishan, M. R.; Fernandez, C. A.; Dalgarno, S. J.; McGrail, P. B.; Warren, J. E.; Atwood, J. L. *J. Am. Chem. Soc.* **2008**, *130*, 16842. (c) Yamada, T.; Iwakiri, S.; Hara, T.; Kanaizuka, K.; Kurmoo, M.; Kitagawa, H. *Cryst. Growth Des.* **2011**, *11*, 1798.

(8) (a) Sun, L.-B.; Li, J.-R.; Park, J.; Zhou, H.-C. *J. Am. Chem. Soc.* **2012**, *134*, 126. (b) Pham, M.-H.; Vuong, G.-T.; Fontaine, F.-G.; Do, T.-O. *Cryst. Growth Des.* **2012**, *12*, 1008.

(9) Kruk, M.; Jaroniec, M. *Chem. Mater.* **2001**, *13*, 3169.

(10) Boettcher, S. W.; Fan, J.; Tsung, C. K.; Shi, Q.; Stucky, G. D. *Acc. Chem. Res.* **2007**, *40*, 784.

(11) Tsuruoka, T.; Furukawa, S.; Takashima, Y.; Yoshida, K.; Isoda, S.; Kitagawa, S. *Angew. Chem., Int. Ed.* **2009**, *48*, 4739.

(12) Yanai, N.; Granick, S. *Angew. Chem., Int. Ed.* **2012**, *51*, 5638.

(13) (a) Ma, L.; Falkowski, J. M.; Abney, C.; Lin, W. *Nat. Chem.* **2010**, *2*, 838. (b) Liu, D.; Xie, Z.; Ma, L.; Lin, W. *Inorg. Chem.* **2010**, *49*, 9107.

(14) Nijem, N.; Veyan, J.-F.; Kong, L.; Wu, H.; Zhao, Y.; Li, J.; Langreth, D. C.; Chabal, Y. J. *J. Am. Chem. Soc.* **2010**, *132*, 14834.